



Fingolimod Augments Monomethylfumarate Killing of GBM Cells

Paul Dent^{1*}, Laurence Booth^{1*}, Jane L. Roberts¹, Andrew Poklepovic² and John F. Hancock³

¹ Departments of Biochemistry and Molecular Biology, Virginia Commonwealth University, Richmond, VA, United States, ² Departments of Medicine, Virginia Commonwealth University, Richmond, VA, United States, ³ Department of Integrative Biology and Pharmacology, University of Texas Health Science Center, Houston, TX, United States

OPEN ACCESS

Edited by:

Liam Chen,
Johns Hopkins University,
United States

Reviewed by:

Seunggu Jude Han,
Oregon Health & Science University,
United States
Pierpaolo Peruzzi,
Brigham and Women's Hospital,
Harvard Medical School,
United States

*Correspondence:

Paul Dent
paul.dent@vcuhealth.org
Laurence Booth
laurence.booth@vcuhealth.org

Specialty section:

This article was submitted to
Neuro-Oncology and Neurosurgical
Oncology,
a section of the journal
Frontiers in Oncology

Received: 25 October 2019

Accepted: 08 January 2020

Published: 28 January 2020

Citation:

Dent P, Booth L, Roberts JL,
Poklepovic A and Hancock JF (2020)
Fingolimod Augments
Monomethylfumarate Killing of GBM
Cells. *Front. Oncol.* 10:22.
doi: 10.3389/fonc.2020.00022

Previously we demonstrated that the multiple sclerosis drug dimethyl fumarate (DMF) and its plasma breakdown product MMF could interact with chemotherapeutic agents to kill both GBM cells and activated microglia. The trial NCT02337426 demonstrated the safety of DMF in newly diagnosed GBM patients when combined with the standard of care Stupp protocol. We hypothesized that another multiple sclerosis drug, fingolimod (FTY720) would synergize with MMF to kill GBM cells. MMF and fingolimod interacted in a greater than additive fashion to kill PDX GBM isolates. MMF and fingolimod radiosensitized glioma cells and enhanced the lethality of temozolomide. Exposure to [MMF + fingolimod] activated an ATM-dependent toxic autophagy pathway, enhanced protective endoplasmic reticulum stress signaling, and inactivated protective PI3K, STAT, and YAP function. The drug combination reduced the expression of protective c-FLIP-s, MCL-1, BCL-XL, and in parallel caused cell-surface clustering of the death receptor CD95. Knock down of CD95 or over-expression of c-FLIP-s or BCL-XL suppressed killing. Fingolimod and MMF interacted in a greater than additive fashion to rapidly enhance reactive oxygen species production and over-expression of either thioredoxin or super-oxide dismutase two significantly reduced the drug-induced phosphorylation of ATM, autophagosome formation and [MMF + fingolimod] lethality. In contrast, the production of ROS was only marginally reduced in cells lacking ATM, CD95, or Beclin1. Collectively, our data demonstrate that the primary generation of ROS by [MMF + fingolimod] plays a key role, via the induction of toxic autophagy and death receptor signaling, in the killing of GBM cells.

Keywords: fingolimod, dimethyl fumarate, Gilenya, Tecfidera, RAS, glioblastoma, microglia

INTRODUCTION

Glioblastoma multiforme (GBM) remains an incurable malignancy, with a median survival of ~14 months from initial presentation (1). There are several issues with developing new effective GBM therapeutics; e.g., the blood brain barrier often prevents the full therapeutic dose of many drugs reaching a brain-localized tumor; the brain is also an immunologically privileged environment that results both in a lack of checkpoint immunotherapy efficacy but also in an environment that contains activated brain associated macrophages, the microglia, which promote the growth,

invasion, and survival of GBM cells (2–6). In the specific instance of brain tumors, whether metastatic disease or GBMs, activated microglia have a symbiotic relationship with tumor cells, each producing growth factors and cytokines that reinforces the malignant phenotype of the tumor cells (7, 8). Thus, one approach to treat tumors localized in the brain would be to break the symbiotic positive relationship between the microglia and the tumor cells.

Multiple sclerosis is a disease in which brain and spinal cord axons undergo demyelination in part due to the actions of an auto-immune disease (9, 10). Activated T cells can enter the CNS where they cause inflammation that promotes additional demyelination, that in turn attracts macrophages that enhance the inflammatory response. In the past 10 years two novel therapeutic agents have been approved for the treatment of relapsing remitting MS: Gilenya® (fingolimod, FTY720) and Tecfidera® (dimethyl-fumarate, DMF) (11, 12). Both drugs are administered orally (PO). Fingolimod is an analog of sphingosine-1-phosphate (S1P), with a plasma C max of ~150 nM. Fingolimod is taken up and phosphorylated before it then acts in an autocrine fashion to activate S1P receptors; receptor activation results in receptor internalization and its proteolytic destruction (13, 14). This results in reactive T cells not migrating to the site of CNS inflammation, and a reduction in disease sequelae. DMF is rapidly metabolized in the plasma of patients to monomethyl-fumarate (MMF) and has a C max in plasma of ~15 μM, with an approximate steady state tissue and plasma concentration of 5 μM. Most laboratory-based oncology studies have used DMF, not MMF, and in over 90% of all publications have used the drug above the clinically relevant range, and the range recommended by the drug makers, Biogen (15, 16). Thus, very little is known about the “real” biology of MMF. For example, high concentrations of DMF, e.g., 30–100 μM, can rapidly increase expression of the anti-oxidant enzymes NRF2 and HO-1 in tumor cells (17, 18). However, in our hands, using MMF at a clinically relevant concentration of 5 μM, no alterations in NRF2 or HO-1 expression were observed in a genetically diverse set of primary human GBM cells. At supra-physiologic concentrations DMF can suppress the inflammatory biology of microglia and astrocytes (19).

The present studies were performed to determine whether the multiple sclerosis medications fingolimod and MMF interact to kill GBM cells and to determine some of the molecular mechanisms by which killing occurs. Our data strongly argue that ATM-AMPK, CD95-caspase 8, and reactive oxygen species signaling play key roles in the killing efficacy of the drug combination.

Abbreviations: ERK, extracellular regulated kinase; PI3K, phosphatidyl inositol 3 kinase; ca, constitutively active; dn, dominant negative; ER, endoplasmic reticulum; AIF, apoptosis inducing factor; AMPK, AMP-dependent protein kinase; mTOR, mammalian target of rapamycin; JAK, Janus Kinase; STAT, Signal Transducers and Activators of Transcription; MAPK, mitogen activated protein kinase; PTEN, phosphatase and tensin homolog on chromosome ten; ROS, reactive oxygen species; CMV, empty vector plasmid or virus; si, small interfering; SCR, scrambled; IP, immunoprecipitation; VEH, vehicle; DMF, dimethyl fumarate; MME, monomethyl fumarate; FTY, FTY720, also known as fingolimod and Gilenya; HDAC, histone deacetylase; GBM, glioblastoma multiforme.

MATERIALS AND METHODS

Materials

MMF was purchased from Selleckchem (Houston, TX). Neratinib was kindly supplied by Puma Biotechnology Inc. (Los Angeles, CA). Fingolimod (FTY720) was purchased from Sigma-Aldrich (St. Louis MO). Trypsin-EDTA, DMEM, RPMI, penicillin-streptomycin were purchased from GIBCOBRL (GIBCOBRL Life Technologies, Grand Island, NY). Other reagents and performance of experimental procedures were as described (15, 20–24). Antibodies used: AIF (5318), BAX (5023), BAK (12105), BAD (9239), BIM (2933), BAK1 (12105), Beclin1 (3495), cathepsin B (31718), CD95 (8023), FADD (2782), eIF2α (5324), P-eIF2α S51 (3398), ULK-1 (8054), P-ULK-1 S757 (14202), P-AMPK S51 (2535), AMPKα (2532), P-ATM S1981 (13050), ATM (2873), ATG5 (12994), mTOR (2983), P-mTOR S2448 (5536), P-mTOR S2481 (2974), ATG13 (13468), MCL-1 (94296), BCL-XL (2764), P-AKT T308 (13038), P-ERK1/2 (5726), P-STAT3 Y705 (9145), P-p65 S536 (3033), p62 (23214), LAMP2 (49067) all from Cell Signaling Technology; P-ULK-1 S317 (3803a) from Abgent; P-ATG13 S318 (19127) from Novus Biologicals.

Methods

Culture, Transfection and *in vitro* Exposure of Cells to Drugs

Primary human GBM isolates were grown in bulk in the flanks of NRG mice; multiple tumor isolates were used throughout the studies in this manuscript. Briefly, tumors were isolated, mechanically macerated, filtered and plated in flasks. Initially, cells were cultured at 37°C (5% (v/v) CO₂) *in vitro* using RPMI supplemented with 0.5% (v/v) fetal calf serum and 10% (v/v) Non-essential amino acids. After ~2 weeks of growth and several passages to remove contaminating mouse fibroblasts, GBM cells were grown in RPMI supplemented with 2.0% (v/v) fetal calf serum and 10% (v/v) Non-essential amino acids. Cells were frozen down in bulk and each vial grown/utilized for a maximum of four weeks of *in vitro* culture. Stem cell variants of the PDX GBM isolates were prepared as described (15, 25–27). Freshly isolated GBM cells and activated microglia directly from the operating room were separated and grown in RPMI supplemented with 2.0% (v/v) fetal calf serum and 10% (v/v) Non-essential amino acids for 6 h, followed by drug exposure and viability assessments made the following day (15, 25–27). Cells were transfected with siRNA molecules or plasmids as described in prior manuscripts (20–24). Cells were transfected with a plasmid to express GFP-K-RAS V12 (0.1 μg) using lipofectamine 2000. Twenty-four hours after transfection, cells were used in assays examining their staining for GFP and RFP.

Detection of Cell Viability, Protein Expression, and Protein Phosphorylation by Immuno-Fluorescence Using a Hermes WiScan Machine

[<https://www.idea-bio.com/> (20–24)]

The text below discussing the Methods we use with the Hermes microscope is reproduced from text published in these review articles (28–30). “The Hermes machine combines

high quality optics with a high-quality computer driven microscope stage, and with dedicated software, e.g., to analyze the immunofluorescent staining intensity of individual cells, i.e., *true* in-cell western blotting. A typical experiment: three independent cultures of a particular tumor cell type are sub-cultured into individual 96-well plates. Twenty-four h after plating, the cells are transfected with a control plasmid or a control siRNA, or with plasmids to express various proteins or validated siRNA molecules to knock down the expression of various proteins. After another 24 h, the cells are ready for drug exposure(s). At various time-points after the initiation of drug exposure, cells are fixed in place with permeabilization. Standard immunofluorescent blocking procedures are employed, followed by incubation of different wells with a variety of validated primary antibodies. The next morning, after washing, fluorescent-tagged secondary antibodies are added to each well; in general, we have found that using more than two tagged antibodies in each well-results in poorer data/image quality. After 3 h of incubation, the secondary antibody is removed, the cells washed again, and are hydrated with phosphate buffered saline prior to microscopic examination. Based on the experiment, cells are visualized at either 10X magnification for bulk assessments of immunofluorescent staining intensity or at 60X magnification for assessments of protein or protein-protein co-localization (**Supplemental Figure 1**).

“For studies at 10X magnification, the operator selects which fluorescent antibody will be assessed first, i.e., in the red or green channel, and then focuses the microscope in a vehicle control transfection control well. The operator then outlines for the computer controlling the microscope “what is a cell.” In other words, the operator manually inputs the criteria for each specific tumor cell line segregating away detection of what is obvious debris or a staining artifact. The operator then sets how many cells per well are to be assessed for their immunofluorescent staining intensity; we initially selected 40 cells per well but have now moved to assessing 100. The computer/microscope then determines the background fluorescence in the well and in parallel randomly determines the mean fluorescent intensity of those 100 cells; the operator is provided with this mean intensity value. Of note for scientific rigor is that the operator does not personally manipulate the microscope to examine specific cells; the entire fluorescent accrual method is independent of the operator. Once the entire plate has been scanned for one of the secondary antibodies, the second secondary antibody with a different fluorescence range can similarly be used to define the mean intensity value in each well. Once data from the first set of plated cells has been obtained, the second and third sets of plated cells can be processed through the machine. Thus, we obtain three independent sets of fluorescence data from the three individual cultures, with 300 cells under each condition being assessed. Typically, the total expression of a particular protein will be assessed alongside additional staining to define the levels of different phosphorylation sites within the protein, e.g., total ULK1, P-ULK1 S317, P-ULK1 S757. Within these analyses it is also essential to include wells to define invariant protein loading controls, such as the expression level of ERK2 or AKT. For phospho-proteins, data can be presented in two ways,

either bar graphs where the total protein expression/loading is presented alongside changes in phospho-protein levels, or with just bars for the phospho-protein fluorescence data corrected for the amount of protein expression, i.e., the stoichiometry of protein phosphorylation. For proteins whose total expression changes after drug exposure, the use of invariant total ERK2 or total AKT expression is used instead as a loading control. Usually, alongside our numeric bar graph data, we also present images of stained cells, taken at 60X magnification, which visually reveal the extent of protein over-expression or of protein knock down. The Hermes microscope has also proved very useful at examining protein-protein interactions at 60X magnification. Three to four images of cells stained in the red and green fluorescence channels are taken for each treatment/transfection/condition. Images are ~4MB sized files. Images are merged using Adobe Photoshop. The image intensity and contrast is then *post-hoc* altered in an identical fashion inclusive for each group of images/treatments/conditions, so that the image with the weakest intensity is still visible to the naked eye for publication purposes but also that the image with the highest intensity is still within the dynamic range, i.e., not over-saturated.”

“At present, many laboratories still utilize traditional western blotting with secondary antibodies conjugated to luciferase, with enhanced chemiluminescence and X-ray film as a read-out; this approach has a limited dynamic range and for the 21st Century lacks sufficient rigor. Other laboratories with access to fluorescent imagers such as the Odyssey system use SDS PAGE with fluorescent tagged secondary antibodies, and these systems have a 5- to 6-log dynamic range. The Odyssey system can, at a gross level, also perform in-cell immunoblotting including co-staining in the red and green fluorescence channels. All of the above procedures require a considerable amount of operator input, including the isolation, lysis, clarification, and loading of proteins onto an SDS PAGE gel, followed by transfer to immobilon. This creates inherent errors in defining small drug-induced alterations to expression and phosphorylation; these are all processing stages where the rigor of the experiment can be compromised. Our use of the Hermes system abolishes all of the intermediate steps as cells are fixed *in situ*. Furthermore, unlike traditional SDS PAGE, the proteins retain their native conformations which for a number of proteins, e.g., detecting changes in chaperone conformation cause by drug exposures, presented data that could not have been obtained using traditional SDS PAGE. Thus, the in-cell assessments of altered phosphorylation or expression using the Hermes microscope provide data with more rigor and a much lower standard deviation difference, permitting changes of 20–30% intensity to be assessed for statistical significance.”

“An additional benefit of using the Hermes system is that it promotes a greater level of rigorous non-manipulatable data. As mentioned earlier, the cells are fixed in place and stained, and then once the machine has been set to recognize the morphology of any specific tumor cell type, the role of the operator has ended. Data is obtained by the machine in a random fashion examining cell staining intensities wherever it detects cells; the operator cannot skew their data by plating more cells in one well-compared to another, or by picking certain cells to scan, leaving other cells out. We believe that our approach using

the Hermes WiScan microscope, or with similar computer-controlled microscope products, should become the standard of approach for immunoblotting/immunofluorescence work.”

Assessment of ROS

“Cells were treated with the drugs and 15 min prior to the indicated time point the media was removed and cells incubated with diacetate dihydro-DCF-DA (5 μ M) (20–24). Fluorescence measurements were obtained 15 min after DCFH-DA addition with a Vector 3 plate reader. Data are presented corrected for basal fluorescence of vehicle-treated cells at each time point and expressed as the arbitrary units provided by the plate reader/the increase in ROS levels.”

Animal Studies

Studies were performed under VCU IACUC protocol AD20008. Animals, $n = 3$ per group, were treated for 14 days with vehicle control (cremophore QD Days 1–14) or with [fingolimod, FTY 0.6 mg/kg + DMF, 75 mg/kg]. For both drugs, this represents an approximate 3-fold higher dosing than would occur in a human multiple sclerosis patient. Five-micron sections of normal tissues were obtained, and H&E staining performed to detect any changes in tissue morphology. No alteration in animal body mass was observed comparing vehicle control treated and [FTY + DMF] treated mice (not shown).

Data Analysis

Comparison of the effects of various treatments (in triplicate three times) was using one-way ANOVA and a two tailed Student's *t*-test. Statistical examination of *in vivo* animal survival data utilized a two tailed Student's *t*-test and log rank statistical analyses between the different treatment groups. Differences with a $p < 0.05$ were considered statistically significant. Experiments are the means of multiple individual points from multiple experiments (\pm SEM).

RESULTS

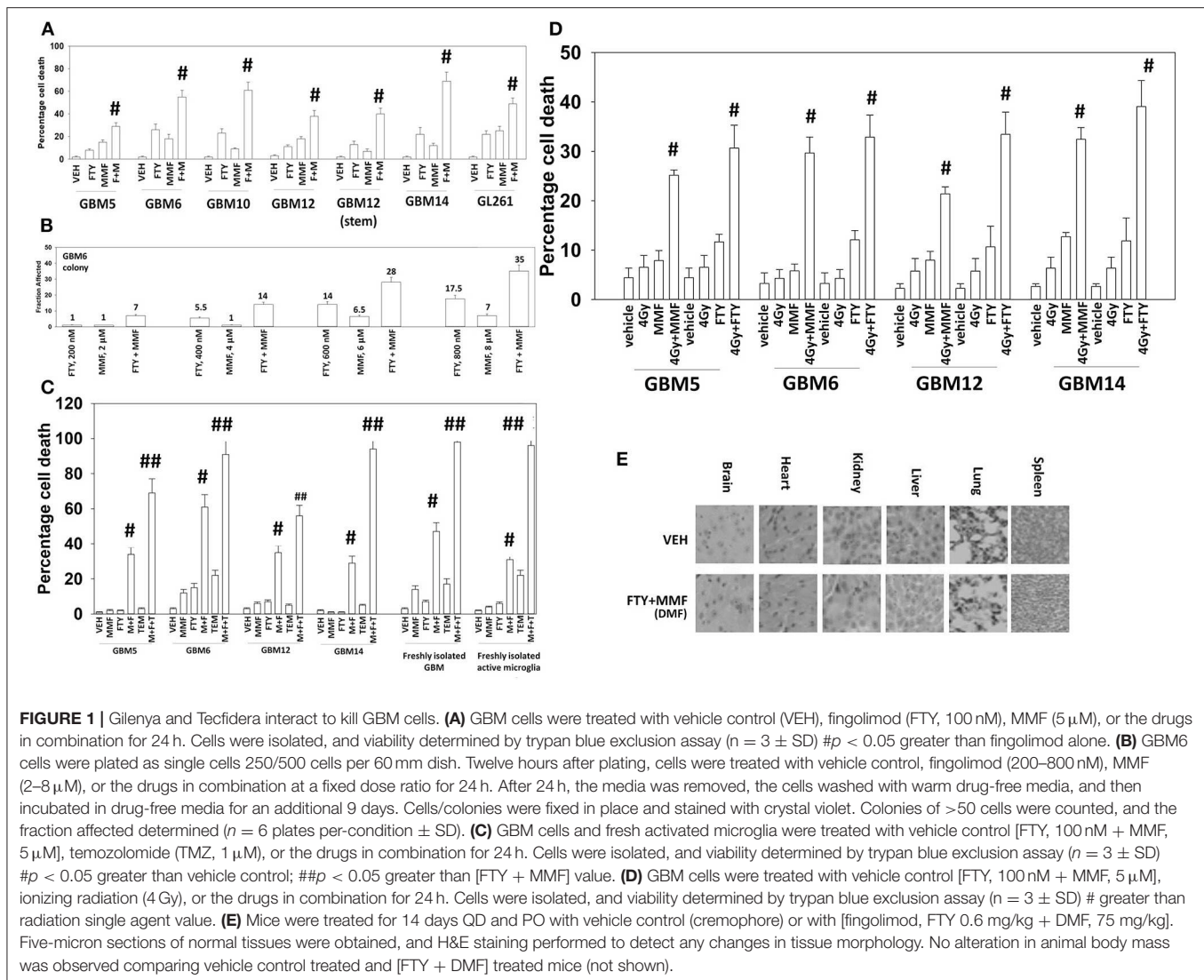
The Mayo clinic-derived and characterized PDX GBM cells are grown in bulk *in vivo* to maintain their tumorigenic biology and invasive characteristics, and the present studies used multiple isolates from different GBM5, GBM6, GBM12, and GBM14 tumors/mice *in vitro*. Fingolimod and MMF at physiologic concentrations interacted in an additive to greater than additive fashion to kill a genetically diverse group of primary and established GBM isolates and GBM stem cells (**Figure 1A**). Similar killing data were obtained using colony formation assays (**Figure 1B**). The combination of [MMF + fingolimod] enhanced the lethality of the standard of care drug temozolomide against GBM cells, and also against a fresh primary GBM isolate with its associated activated microglia (**Figure 1C**). Prior studies have demonstrated that the [MMF + fingolimod] combination could kill other primary GBM isolates, TNBC breast cancer cell lines, NSCLC isolates, ovarian isolates and sarcoma isolates (15). Both MMF and fingolimod radiosensitized our GBM isolates (**Figure 1D**). We next determined whether animals exposed to fingolimod and MMF in combination would exhibit any

normal tissue toxicities. Animals were treated daily for 14 days with drug doses \sim 3 times higher than those of either drug in multiple sclerosis patients. Supra-physiologic doses of the drugs *in vivo* did not cause damage to “normal tissues” in the mouse (**Figure 1E**). This finding argues that the [MMF + fingolimod] drug combination will likely be “safe” in a human cancer patient.

We selected the PDX models GBM6 and GBM14 for further in-depth analyses. The GBM6 isolate expresses the truncated constitutively active ERBB1 vIII and the GBM14 isolate lacks PTEN expression. In many prior experimental therapeutics studies, we have performed agnostic screening analyses following exposure of cancer cells to drugs using the Hermes wide-field microscope. Using fluorescence intensity imaging of individual cells, we define the changes in the expression and phosphorylation of multiple signal transduction proteins (20, 21, 24, 31). Signaling by ERK1/2, AKT, mTOR, p70 S6K, STAT3, and STAT5 was assessed, as was signaling by ATM, the AMPK and eIF2 alpha. Studies also closely examined the regulation of autophagy, measuring the levels of Beclin1, ATG5 and the phosphorylation of ULK1 and ATG13. The levels of multiple cytoprotective proteins were assessed including MCL-1, BCL-XL, and c-FLIP-s.

In GBM6, but not GBM14, the drugs combined to further activate ATM and AMPK; in several prior studies using different drug combinations we have delineated an ATM-AMPK-ULK1-ATG13 pathway that promotes autophagosome formation (**Figures 2A,B**) (20, 21, 24, 31). In GBM14 cells, fingolimod as a single agent strongly activated ATM-AMPK signaling. In both cell lines FTY720 and MMF interacted to promote ULK-1 S317 phosphorylation; S317 is a site targeted by the AMPK and elevated S317 phosphorylation equates to ULK-1 kinase activation. This was associated with enhanced ATG13 S318 phosphorylation; elevated S318 phosphorylation is a key trigger event to initiate autophagosome formation. The [MMF + fingolimod] combination rapidly inactivated mTORC1, mTORC2, AKT, ERK1/2, p70 S6K, STAT3/5, and NF κ B. Inactivation of mTORC1 and mTORC2 results in ULK-1 S757 dephosphorylation that also promotes ULK-1 kinase activity. In both GBM6 and GBM14 cells, the drugs interacted to reduce STAT5 Y694 phosphorylation and in one of the isolates STAT3 Y705 phosphorylation. In one isolate, the drugs also interacted to reduce NF κ B S536 phosphorylation. As judged by elevated PKR-like endoplasmic reticulum kinase (PERK) phosphorylation and elevated eIF2 α S51 phosphorylation, FTY720 caused a strong endoplasmic reticulum stress response. In both isolates, the drug combination also reduced the expression of the caspase 8/10 inhibitor c-FLIP-s, that potentially could facilitate death receptor signaling.

We have recently demonstrated that the irreversible ERBB1/2/4 inhibitor neratinib could down-regulate the expression of RAS proteins, and based on this data and the fact that phosphorylated fingolimod causes sphingosine-1-phosphate receptor 1 internalization and degradation, we wished to determine whether this drug could act upon RAS proteins in GBM cells, in a manner similar to neratinib (20, 21, 24, 31). In GBM6 cells, that express an NH2-terminal truncated active ERBB1 vIII [fingolimod + MMF], caused intracellular clustering



of the receptor; unlike fingolimod, our positive control neratinib increased clustering followed later by reduced expression of the receptor (**Figure 3A**). In GBM6 cells, fingolimod as a single agent could reduce the total expression of both wild type K- and N-RAS proteins (**Figure 3B**). To confirm this finding via a different approach, we transfected GBM6 cells with a plasmid to express K-RAS V12-GFP. In a manner similar to the data for ERBB1 vIII in Panel A, fingolimod caused intracellular vesicularization of K-RAS V12-GFP, that was maintained for 8 h (**Figure 3C**). In contrast, the positive control neratinib initially caused RAS vesicularization but at later times reduced the levels of GFP+ fluorescence. Finally, we wished to determine whether the effect of fingolimod on RAS vesicularization was specific only in GBM cells. PANC1 pancreatic cancer cells express a mutant K-RAS protein. PANC1 cells were transfected with plasmids to express K-RAS V12-GFP and K-RAS V12-RFP. In these cells, fingolimod appeared to cause greater levels of RAS vesicularization than were observed in the GBM

cells (**Figure 3D**). In contrast to data from GBM cells, after 8 h of drug exposure, fingolimod reduced GFP+ and RFP+ fluorescence levels.

Additional descriptive studies were performed to further delineate the responses of GBM cells to [MMF + fingolimod]. After drug exposure, the expression of proteins generally considered to be protective against toxic stresses including MCL-1, BCL-XL, c-FLIP-s declined whereas the expression of proteins that facilitated autophagosome formation, ATG5 and Beclin1, increased (**Figures 2A,B, 4A**). The expression of β -catenin declined. High non-physiologic concentrations of DMF (>5 μ M) have been proposed to increase the expression of NRF2 and HO-1 that are proteins which in a broad sense will act to suppress reactive oxygen species (ROS) production. ROS production is essential for the activation and activities of many different types of immune cell. Reactive oxygen also activates cytosolic ATM (32). Lower concentrations of MMF rapidly enhanced the production of ROS in GBM cells that

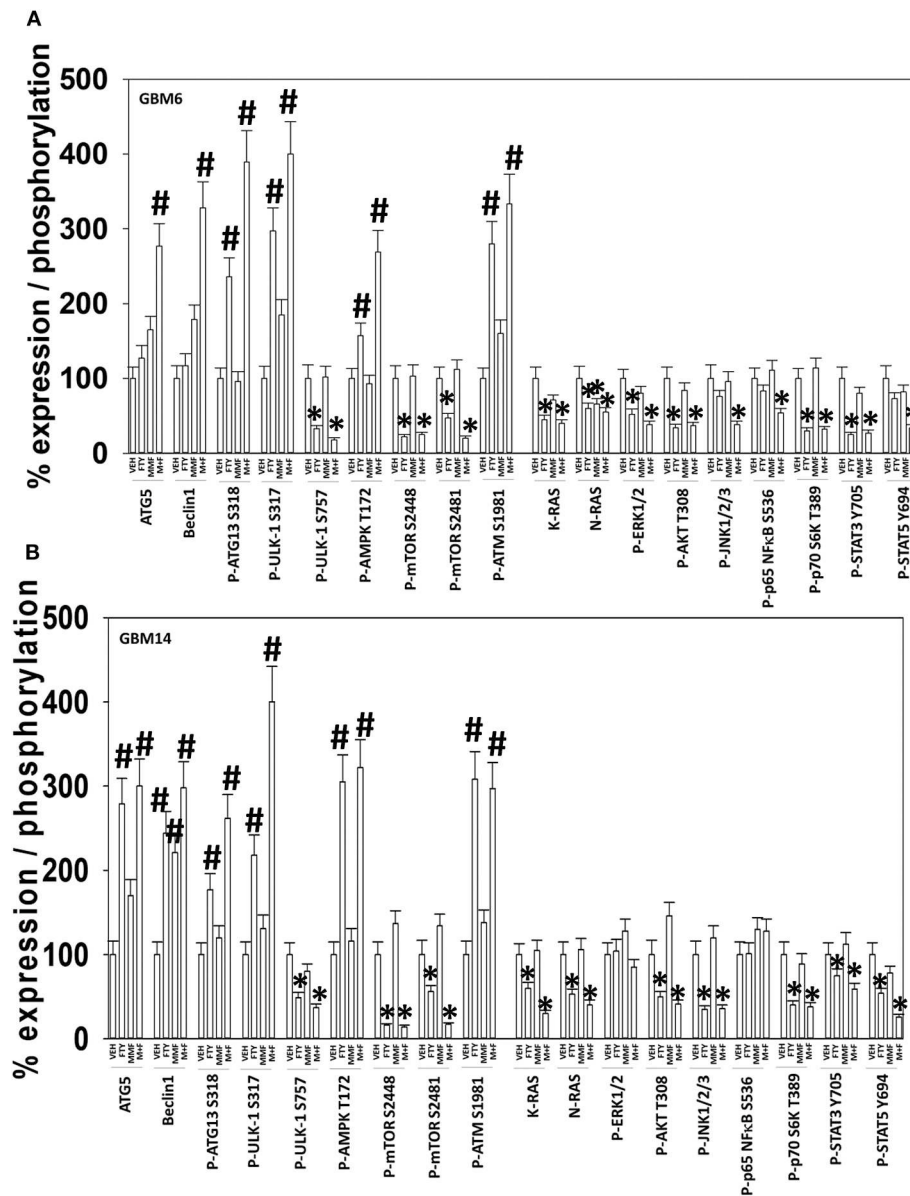
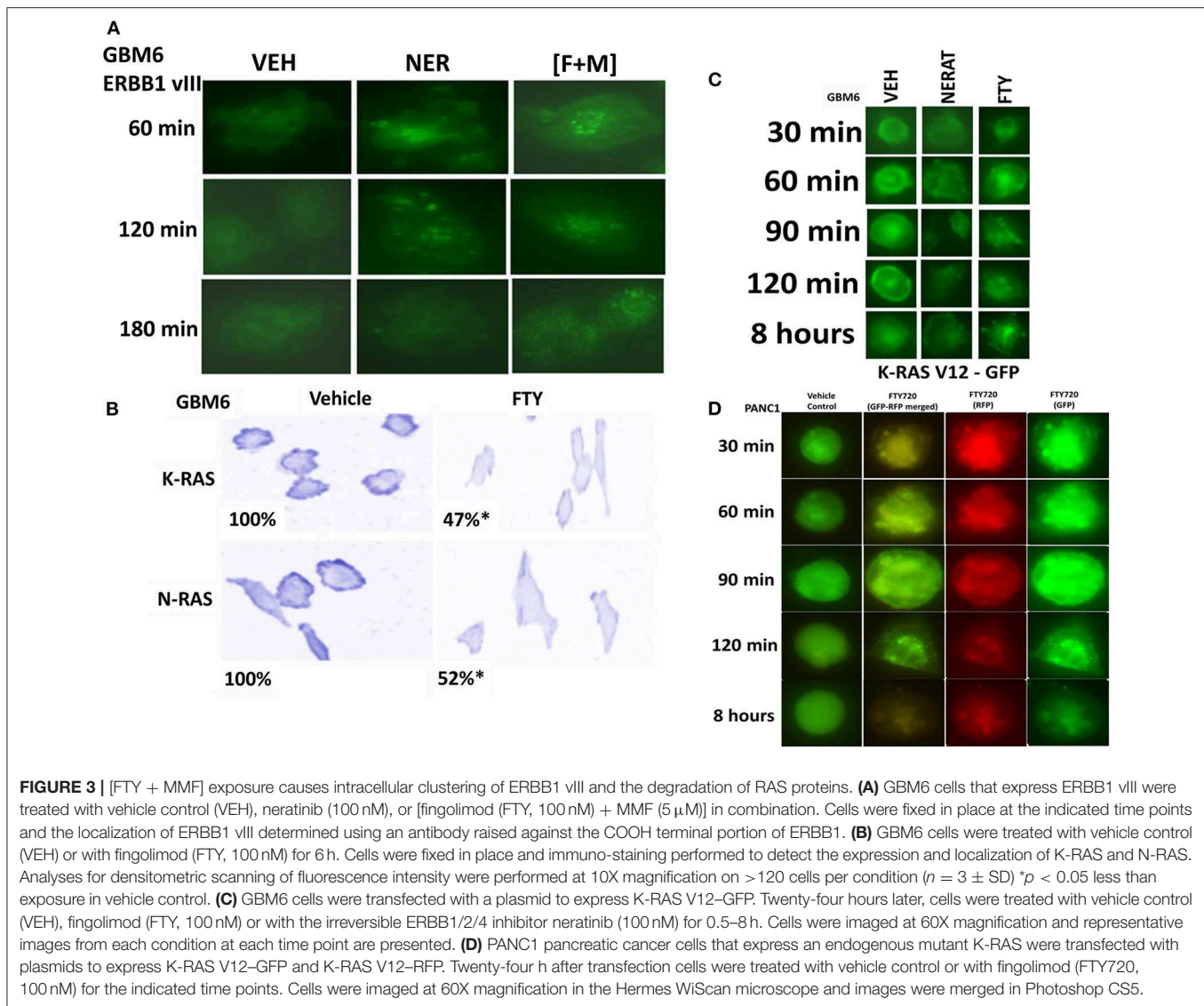


FIGURE 2 | [FTY + MMF] exposure enhances ER stress signaling, causes DNA damage, and inactivates multiple protective signaling pathways. **(A)** GBM6 and **(B)** GBM14 cells were treated with vehicle control (VEH), fingolimod (FTY, 100 nM), MMF (5 μ M), or the drugs in combination for 6 h. Cells were fixed in place and immuno-staining performed to detect the total expression and phosphorylation of the noted proteins. Analyses for densitometric scanning of fluorescence intensity were performed at 10X magnification on >120 cells per condition, in a random fashion in a Hermes WiScan machine ($n = 3 \pm$ SD) * $p < 0.05$ less than exposure in vehicle control; # $p < 0.05$ greater than exposure in vehicle control.

remained constant for almost 4 h (**Figure 4B**). As a single agent fingolimod, also at a clinically relevant concentration (100 nM), modestly and transiently increased ROS production. When the drugs were combined, fingolimod significantly enhanced the ability of MMF to generate ROS over the 4-h time course. Over-expression of thioredoxin (TRX) or superoxide dismutase 2 (SOD2) quenched ROS production and significantly reduced [MMF + fingolimod] lethality, as did expression of activated MEK1, dominant negative $\text{I}\kappa\text{B}$ S32A S36A, and treatment

with the JNK inhibitory peptide (**Figure 4C**, not shown). In cells treated with [MMF + fingolimod], despite exhibiting elevated ROS levels, no compensatory survival alterations in the expression of NRF2 or HO-1 were observed (not shown).

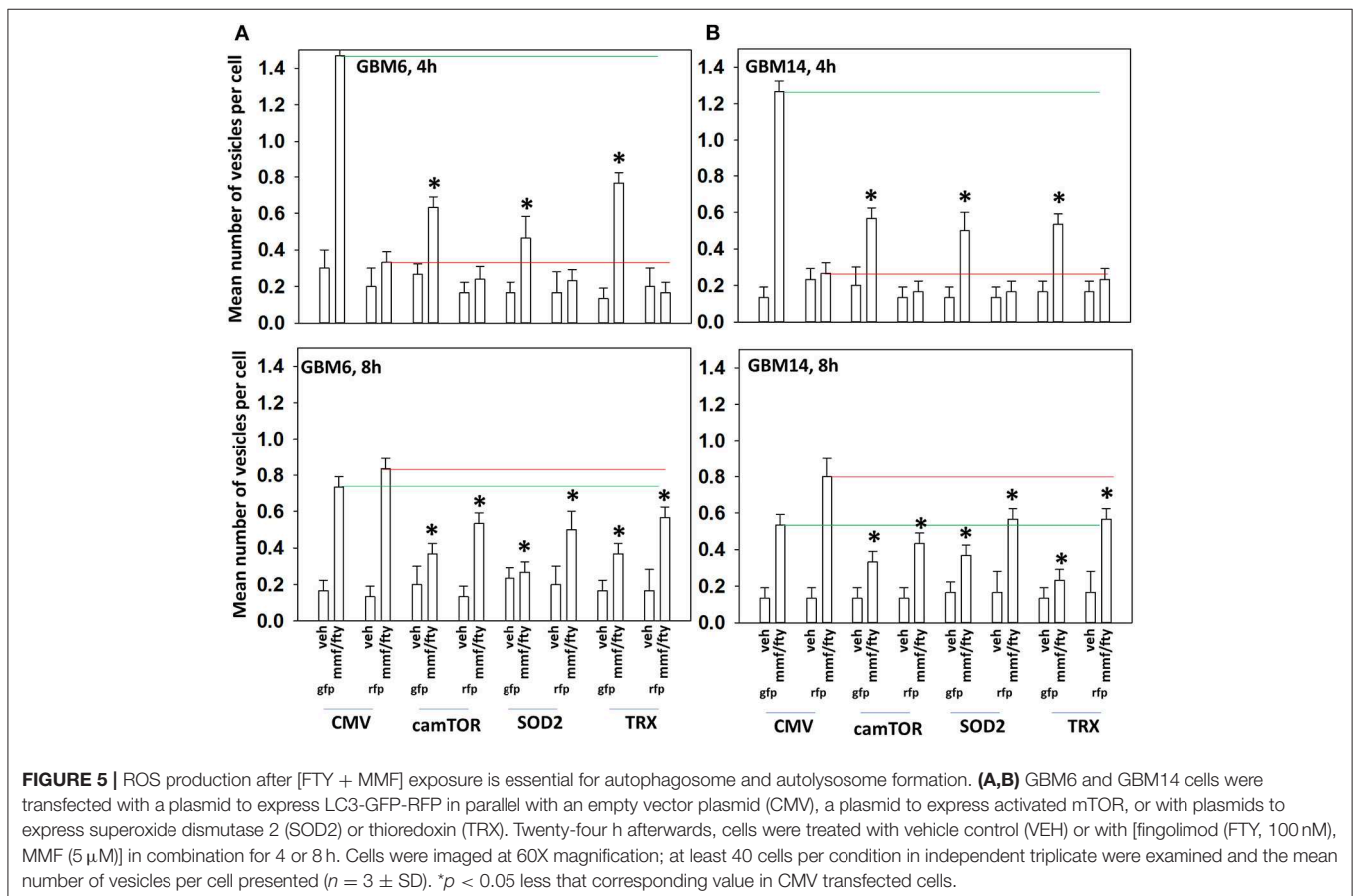
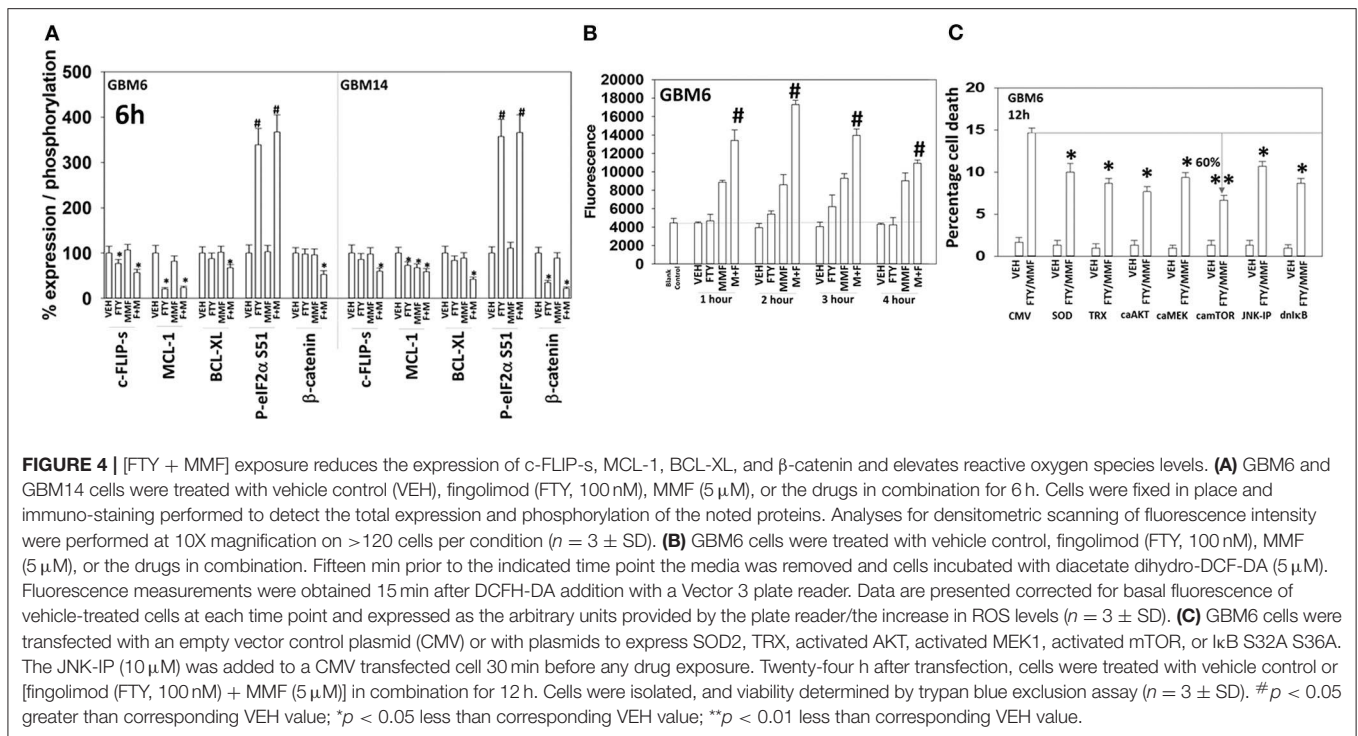
In **Figure 2** we observed that [MMF + fingolimod] inactivated mTOR and increased the phosphorylation of ATG13, all strongly suggesting that the drug combination was promoting autophagosome formation. GBM cells were transfected to express the fusion protein LC3-GFP-RFP which permits the

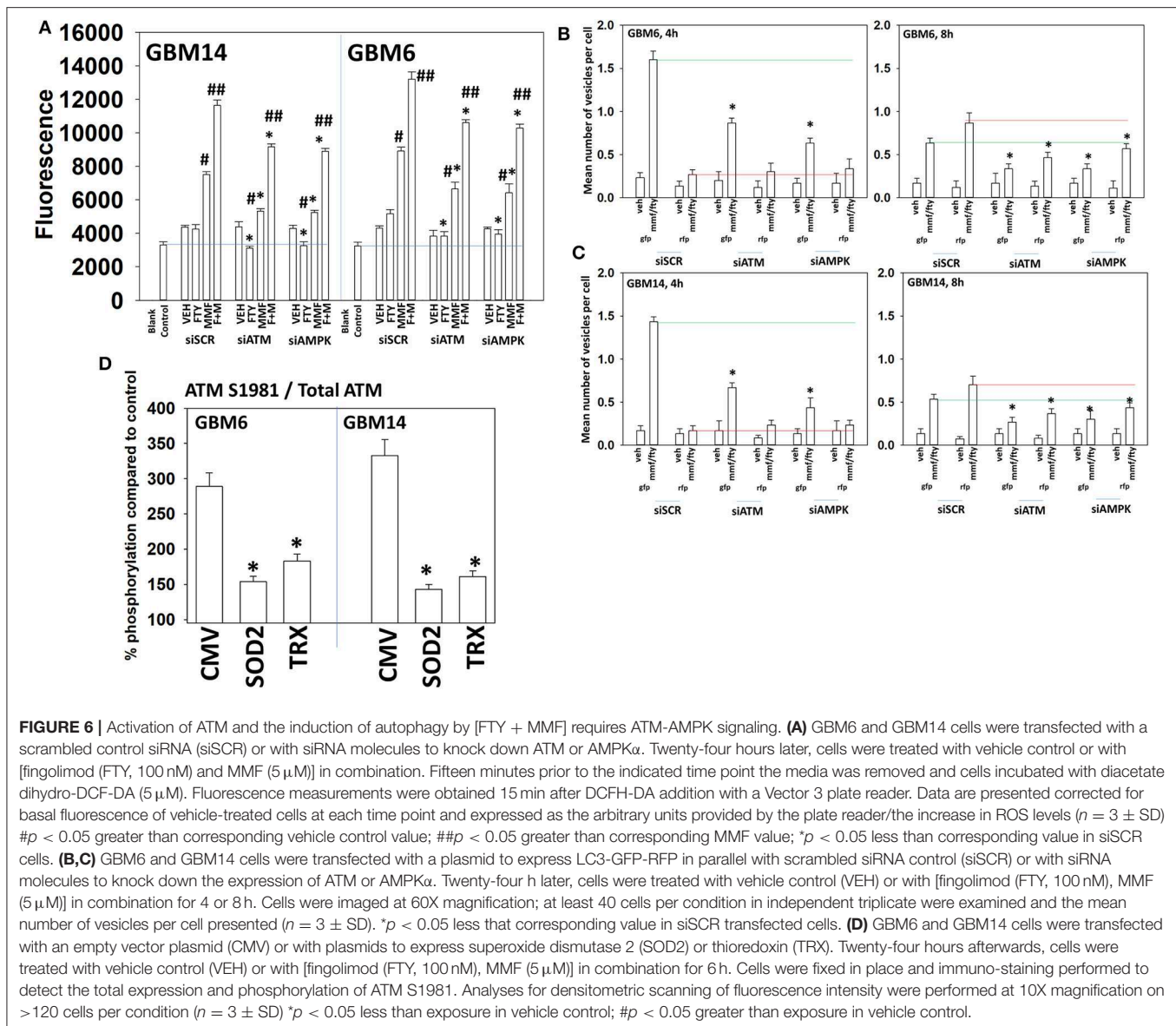


detection over a time course of autophagosomes (GFP+ RFP+) and autolysosomes (RFP+); i.e., autophagic flux. Treatment of cells with [MMF + Fingolimod] increased the levels of autophagosomes followed temporally later by the formation of autolysosomes, arguing that the drug combination was stimulating autophagic flux (Figures 5A,B). Over-expression of TRX or SOD2 to quench reactive oxygen species or a mutant active form of mTOR to inactivate the kinase upstream of ATG13, ULK1, significantly reduced the drug-stimulated elevations in the levels of autophagosomes and autolysosomes.

ATM in the cytosol can be activated by reactive oxygen species whereas ATM associated with DNA in the nucleus can be activated by DNA damage (32). Figure 2 demonstrated that fingolimod activated ATM but data in Figure 4 demonstrated that fingolimod weakly elevated reactive oxygen species levels. This suggests fingolimod may be causing a DNA damage-induced activation of ATM. And, as an HDAC inhibitor,

fingolimod has the potential to cause DNA damage. Knock down of ATM or AMPK α modestly, though significantly, reduced amount of ROS generated by MMF and by [MMF + fingolimod] 2 h after exposure, each by \sim 20% (Figure 6A). Knock down of ATM or AMPK α significantly reduced the ability of the drug combination to stimulate autophagosome formation after 4 h by 45–90% (Figures 6B,C). Although evidence from Figures 2, 4 would argue that reactive oxygen species plays a secondary role in the regulation of ATM activity, over-expression of TRX or SOD2 significantly reduced the drug combination-stimulated phosphorylation of ATM S1981 \sim 50–60% (Figure 6D). Collectively, the data in Figures 2–6 demonstrate that the initial sharp increase in ROS generation caused by [MMF + fingolimod] exposure is essential for robust ATM activation and for autophagosome formation, and that ROS generation is upstream of ATM activation and autophagy. Future studies will be required to explore the



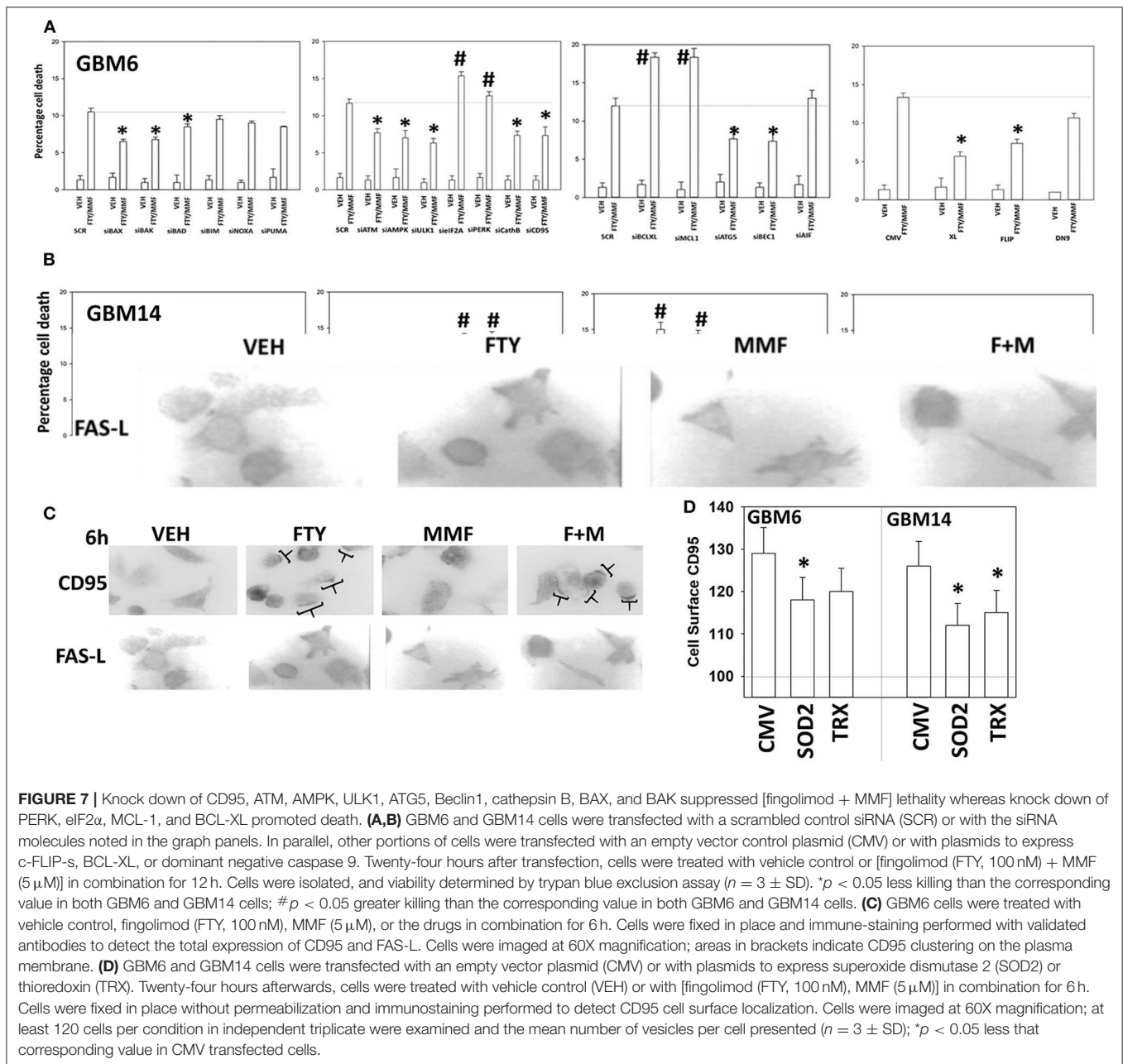


role of nuclear DNA damage in the activation of ATM after drug exposure.

Based on the data in **Figures 1–6**, using molecular tools, we next performed additional semi-descriptive studies designed ultimately to define the key protein regulators/pathways of viability after [MMF + fingolimod] exposure. Cell killing deliberately measured after only 12 h, i.e., the numeric values of percentage cell death are relatively low but are performed at this time point so as to define those key proteins/pathways who play a *primary* role in the killing processes. Proteins that were congruent in both PDX isolates for regulating tumor cell killing by the drug combination were: [BAX, BAK, BAD; MCL-1, BCL-XL] that could be considered as a mitochondrial apoptosis regulatory pathway; [ATM, AMPK, ULK-1, ATG5, Beclin1, Cathepsin B] that could be considered as an autophagy/lysosomal pathway; [CD95, c-FLIP-s] as a death receptor pathway feeding

into the apoptosis pathway; and enhanced [PERK, eIF2 α] ER stress signaling that promotes cell survival (**Figures 7A,B**). With respect to death receptor signaling, fingolimod, but not MMF, caused plasma membrane clustering of CD95, indicative of death receptor activation (**Figure 7C**). Over-expression of the reactive oxygen species quenching enzymes TRX or SOD2 modestly, though significantly, reduced CD95 plasma membrane levels (**Figure 7D**). Tyrosine phosphorylation of CD95 is known to play a key role in its activation (33). Tyrosine phosphatases are potentially inhibited by reactive oxygen species and thus inhibition of PTPases by ROS may represent a mechanism of CD95 activation.

As presented in **Figure 2**, knock down of PERK or eIF2 α enhanced [MMF + fingolimod] lethality, implying endoplasmic reticulum stress signaling was protective. Hence, we next determined whether other endoplasmic reticulum



stress pathways regulated the survival response to [MMF + fingolimod] treatment. Knock down of the IRE1-XBP1 pathway or the ATF6 pathway, in a manner like knock down of the PERK-eIF2 α pathway, enhanced killing GBM6 and GBM14 cells (**Figure 8**). In GBM6 cells, knock down of the ER stress pathways enhanced MMF lethality, whereas in GBM14 no enhancement occurred. In GBM6 cells, fingolimod lethality was not altered by knock down of the ER stress pathways whereas in the GBM14 cells, killing was modestly enhanced. Whether PTEN functionality (GBM14) or ERBB1 vIII expression (GBM6) specifically alters the role of ER stress signaling

in survival will require studies beyond the scope of the present manuscript.

Glioblastoma is a highly invasive tumor type, and one signaling pathway that can interact with ERBB1-RAS signaling to promote tumor cell migration and invasion is the Hippo Pathway (34). The downstream effectors of this pathway, YAP and TAZ, are active when dephosphorylated, and in the nucleus where they act as co-transcription factors (35). Treatment of GBM6 and GBM14 cells caused a biphasic regulation of YAP and TAZ phosphorylation, as well as of their upstream kinases LATS1/2 and of docking

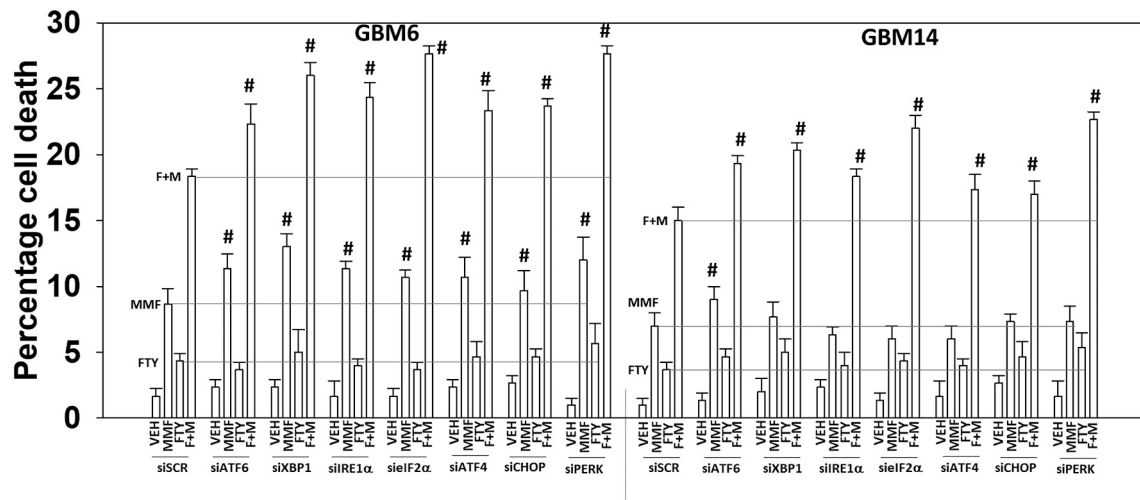


FIGURE 8 | Endoplasmic reticulum stress signaling plays a protective role against [MMF + fingolimod] exposure. GBM6 and GBM14 cells were transfected with a scrambled siRNA control (siSCR) or with the indicated siRNA molecules to knock down the expression of proteins that regulate ER stress pathways. Twenty-four hours after transfection, cells were treated with vehicle control, MMF (5 μ M), fingolimod (100 nM), or the drugs in combination for 12 h. Cells were isolated, and viability determined by trypan blue exclusion assay ($n = 3 \pm$ SD). # $p < 0.05$ greater than corresponding value in siSCR cells.

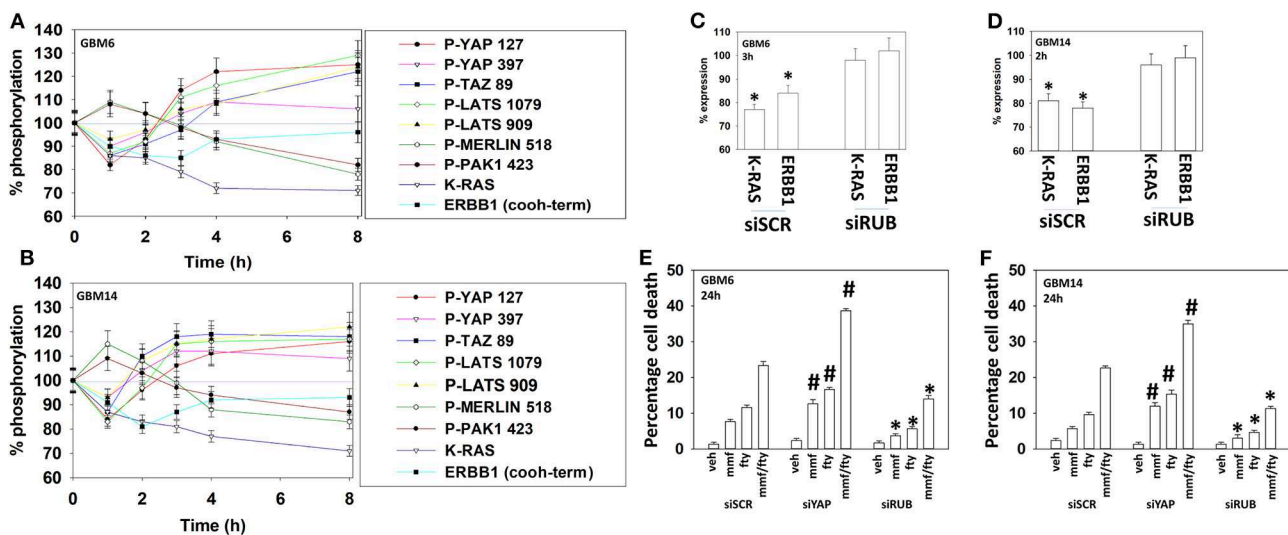


FIGURE 9 | Fingolimod causes bi-phasic activation followed by inactivation of YAP and TAZ. **(A,B)** GBM6 and GBM14 cells were treated with vehicle control or with fingolimod (100 nM). At each time point over the 0–8 h time course cells were fixed in place and immunostaining performed to determine the fluorescence intensity levels of: total YAP, total TAZ, total Merlin, total PAK1; total LATS1; P-YAP S127; P-YAP S397; P-TAZ S89; P-LATS T1079; P-LATS S909; P-Merlin S518; P-PAK1 T423; total ERBB1; and total K-RAS from 10X magnification images (120 cells per condition, $n = 3 \pm$ SD). **(C,D)** GBM6 and GBM14 cells were transfected with a scrambled control siRNA (siSCR) or with an siRNA to knock down the expression of Rubicon. Twenty-four h after transfection cells were treated with vehicle control or with fingolimod (100 nM). At each time point over the 0–8 h time course cells were fixed in place and immunostaining performed to determine the fluorescence intensity levels of: total ERBB1; total K-RAS from 10X magnification images (120 cells per condition, $n = 3 \pm$ SD). * $p < 0.05$ less than vehicle control. **(E,F)** GBM6 and GBM14 cells were transfected with a scrambled control siRNA (siSCR) or with an siRNA to knock down the expression of Rubicon or the expression of YAP. Twenty-four h after transfection cells were treated with vehicle control, fingolimod (100 nM), MMF (5 μ M), or the drugs in combination for 24 h. Cells were isolated, and viability determined by trypan blue exclusion assay ($n = 3 \pm$ SD). * $p < 0.05$ less than corresponding value in siSCR cells; # $p < 0.05$ greater than corresponding value in siSCR cells.

proteins Merlin and PAK1 (**Figures 9A,B**). In both cell types, fingolimod within the first 2 h of exposure initially caused dephosphorylation of YAP, TAZ, and LATS1/2 and increased the phosphorylation of Merlin and PAK1. These

events facilitate the co-transcription factor activities of YAP and TAZ, with Merlin acting to regulate complex formation and downstream signaling from small GTP binding proteins (36). At later times, 3–8 h after exposure, fingolimod caused

the phosphorylation of YAP, TAZ, LATS1/2, and caused the dephosphorylation of Merlin and PAK1. Reduced Merlin phosphorylation enhances the ability of Merlin to act as a docking/chaperone protein bringing LATS1/2 into a closer association with YAP/TAZ, which enhances YAP/TAZ phosphorylation, thereby reducing YAP/TAZ activity (37).

One mechanism of plasma membrane internalization and subsequent protein digestion is called LC3-associated phagocytosis (LAP) (37). Key regulatory proteins in this process include Rubicon and Beclin1; our prior data demonstrated Beclin1 knock down protected cells from [MMF + fingolimod] lethality. Knock down of Rubicon prevented fingolimod from reducing the protein levels of K-RAS and ERBB1 (Figures 9C,D) (38). Knock down of Rubicon reduced the lethality of fingolimod, MMF and the drug combination (Figures 9E,F). In contrast, knock down of YAP enhanced killing by the drugs alone or in combination. These findings argue that reduced YAP phosphorylation caused by fingolimod leads to enhanced killing by the drug and that in cells incapable of LAP-dependent K-RAS/ERBB1 destruction, fingolimod lethality is significantly reduced.

DISCUSSION

The recognized actions of fingolimod and of DMF are to suppress immune system activity such that the host's auto-immune actions against demyelinated nerves, i.e., multiple sclerosis, are reduced. Although both drugs act to reduce the reactivity of the immune system, they do so through different mechanisms. Glioblastoma, for its overall malignancy and its invasion and privileged environment, relies heavily on its symbiotic relationship with activated/reactive microglia. As such, we hypothesized that a combination of the CNS-permeant drugs fingolimod and DMF/MMF could have therapeutic potential in this disease. Prior studies demonstrated that MMF reduced GBM cell invasiveness and enhanced the toxicity of temozolomide and ionizing radiation (15). MMF killed freshly isolated activated human microglia which correlated with reduced IL-6, TGF β , and TNF α production. The MMF and fingolimod combination further reduced, below either agent individually, both GBM and activated microglia viability and their production of cytokines. In animals treated with DMF and fingolimod for 14 continuous days, no obvious damage to normal tissues was observed.

We demonstrated that the drug combination enhanced ATM/AMPK/ULK-1 signaling that corresponded with enhanced ATG13 S318 phosphorylation, as observed in prior therapeutics studies; in one isolate knock down of ATG5 and Beclin1 was protective against drug lethality whereas in the other it was not. Both isolates required the lysosomal protease cathepsin B for complete execution of the tumor cells. The drug combination reduced the protein levels of cytoprotective proteins such as ERBB1 vIII, K-RAS, N-RAS, c-FLIP-s, MCL-1, and BCL-XL. Knock down of CD95 or FADD, or over-expression of c-FLIP-s reduced drug combination killing arguing that the extrinsic pathway played a partial role in the killing process. Knock down

of MCL-1 or BCL-XL enhanced tumor cell death whereas over-expression of BCL-XL was protective as was knock down of BAX, BAK and BAD. This data more definitively supports the drug combination causing mitochondrial dysfunction as a key component of the killing process. Knock down of apoptosis inducing factor significantly protected cells whereas expression of dominant negative caspase 9, i.e., "classic" apoptosis via caspase 3, did not. Alongside the role of cathepsin B, these findings demonstrate that the [MMF + fingolimod] combination kills through non-apoptotic processes.

At non-physiologic DMF/MMF concentrations, an order of magnitude higher than used herein, the drug has been shown to modulate the anti-oxidant response in cells, increasing the expression of NRF2 and HO-1. Because of this data linking DMF/MMF to the anti-oxidant response, we investigated whether MMF and fingolimod interacted to alter ROS levels and whether ROS generation play any role in tumor cell killing. MMF enhanced the production of ROS in GBM cells that was significantly enhanced in a greater than additive fashion by fingolimod. Over-expression of thioredoxin or superoxide dismutase 2 suppressed ROS production and drug combination lethality, yet the drug combination altered neither the levels of TRX and SOD2 expression, nor the levels of NRF2 and HO-1. Over-expression of either TRX or SOD2 significantly reduced the drug-induced phosphorylation of ATM, autophagosome formation and [MMF + fingolimod] lethality whereas the production of ROS was only marginally reduced in cells lacking ATM, CD95, or Beclin1. Thus, the greater than additive induction of ROS by the combination of MMF and fingolimod represents a key primary step in the initiation of the killing process. Further work will be required to define the source(s) of ROS production, e.g., mitochondria.

In many previous manuscripts we have demonstrated that a diverse set of compounds, and chemotherapeutic drug combinations, activate the death receptor CD95. For example, in primary hepatocytes, bile acid-induced CD95 activation can under certain circumstances enhance growth or, alternatively, cell death (39). In tumor cells, CD95 activation appears to only promote cell death. HDAC inhibitors, and fingolimod is an HDAC inhibitor, can increase the expression of CD95 and FAS-Ligand, and whilst [MMF + fingolimod] did not enhance CD95 and FAS-L levels, the drug combination did cause "capping" of CD95 on the cell surface. Genetically manipulated over-expression of TRX or SOD2 only partially reduced the plasma membrane clustering of CD95, arguing that other mechanisms play a more essential role in the process. Additional research will be required to fully define the molecular mechanisms of CD95 activation.

The molecular mechanisms by which [MMF + fingolimod] reduce the expression levels of K-RAS are poorly understood. Our data argued that the drugs reduced K-RAS and ERBB1 levels via Rubicon-dependent LAP followed by autophagic digestion. Clathrin-coated pits and caveolae are also two major endocytic structures which could play roles in RAS/ERBB1 destruction (40). Cholesterol, whose levels are regulated by AMPK signaling via inhibition of acetyl CoA carboxylase, an effect

that also will lower the levels of farnesyl- and geranylgeranyl prenylation substrates, could impact K-RAS prenylation of K-RAS.

Fingolimod exposure initially “activated” YAP and TAZ by causing their dephosphorylation, followed later by enhancing their phosphorylation above baseline, i.e., reducing YAP/TAZ co-transcription factor activity. After fingolimod enters a cell it is phosphorylated where-after it acts in an autocrine fashion binding to S1P receptors. Initially, fingolimod causes receptor activation which is rapidly followed by receptor internalization and receptor degradation. S1P has been shown to reduce YAP phosphorylation and promote invasion, which is congruent with our findings (41, 42). However, when fingolimod has caused destruction of the S1P receptors, we observe increased YAP phosphorylation above basal levels. This suggests there may be a dynamic balance of S1P-dependent regulation of YAP in GBM cells which controls migration and invasion.

A considerable number of studies have used “modern” drug modulators of signal transduction processes in the hope of discovering a new approach to prolong survival of GBM patients. However, the median survival for GBM patients has only marginally improved over the past two decades when these drugs have been available. Checkpoint inhibitory and cellular immunotherapies have yet to exhibit any significant alteration in progression free or overall survival (43, 44). If we cannot enhance the immune system to attack GBM tumor cells, we reasoned, our initial conceptual approach became instead to attack the immune cell-rich soil in which the GBM tumor cells require to grow, thereby suppressing tumor cell growth and invasion, and with the hope that this will also enhance the lethality of standard of care therapeutics.

Our *in vitro* data has confirmed that the [MMF + fingolimod] drug combination acts to suppress the cytokine production and viability of freshly isolated activated human microglia. To our pleasant surprise, this drug combination also effectively killed multiple PDX isolates of human GBM cells, and both MMF and fingolimod enhance the lethality of temozolomide and of ionizing radiation. In addition to these observations was that this drug combination promoted the degradation of RAS proteins and oncogenic receptors such as ERBB1 vIII. Furthermore, the drugs inactivated YAP/TAZ signaling which further reduced viability. Future studies will be required to understand whether [MMF + fingolimod] can suppress GBM tumor growth *in vivo* in parallel with the combination altering cytokine production and

modifying reactive microglia biology, without causing normal tissue toxicity.

DATA AVAILABILITY STATEMENT

All datasets generated for this study are included in the article/**Supplementary Material**.

ETHICS STATEMENT

The animal study was reviewed and approved by Studies were performed per USDA regulations under VCU IACUC protocol AD20008.

AUTHOR CONTRIBUTIONS

PD wrote the manuscript. JH edited the manuscript and provided essential reagents. PD and AP conceptualized the experiments. LB and JR performed the experiments.

FUNDING

Support for the present study was funded from philanthropic funding from Massey Cancer Center, the Universal Inc. Chair in Signal Transduction Research and PHS R01-CA192613 (PD).

ACKNOWLEDGMENTS

Thanks to Dr. J. Martinez (NIEHS, Research Triangle, NC); Dr. H. F. Young and the Betts Family Fund for support in the purchase of the Hermes Wiscan instrument.

DEDICATION

This manuscript is dedicated to the corresponding author’s wife who for the past 6 years, daily, has had to take Gilenya.

SUPPLEMENTARY MATERIAL

The Supplementary Material for this article can be found online at: <https://www.frontiersin.org/articles/10.3389/fonc.2020.00022/full#supplementary-material>

Supplemental Figure 1 | Control data showing protein knock-down or protein over-expression in GBM cells. GBM6 cells were transfected to knock down or to over-express proteins ($n = 3 \pm SD$).

REFERENCES

- Wick W, Osswald M, Wick A, Winkler F. Treatment of glioblastoma in adults. *Ther Adv Neurol Disord.* (2018) 11:1756286418790452. doi: 10.1177/1756286418790452
- Balça-Silva J, Matias D, Carmo AD, Sarmiento-Ribeiro AB, Lopes MC, Moura-Neto V. Cellular and molecular mechanisms of glioblastoma malignancy: implications in resistance and therapeutic strategies. *Semin Cancer Biol.* (2019) 58:130–41. doi: 10.1016/j.semcancer.2018.09.007
- Razpotnik R, Novak N, Curin Šerbec V, Rajcevic U. Targeting malignant brain tumors with antibodies. *Front Immunol.* (2017) 8:1181. doi: 10.3389/fimmu.2017.01181
- Roesch S, Rapp C, Dettling S, Herold-Mende C. When immune cells turn bad-tumor-associated microglia/macrophages in glioma. *Int J Mol Sci.* (2018) 19:E436. doi: 10.3390/ijms19020436
- Schiffer D, Mellai M, Bovio E, Annovazzi L. The neuropathological basis to the functional role of microglia/macrophages in gliomas. *Neurol Sci.* (2017) 38:1571–7. doi: 10.1007/s10072-017-3002-x

6. Poon CC, Sarkar S, Yong VW, Kelly JJP. Glioblastoma-associated microglia and macrophages: targets for therapies to improve prognosis. *Brain*. (2017) 140:1548–60. doi: 10.1093/brain/aww355
7. Ahmed S, Gull A, Khuroo T, Aqil M, Sultana Y. Glial cell: a potential target for cellular and drug based therapy in various CNS diseases. *Curr Pharm Des*. (2017) 23:2389–99. doi: 10.2174/1381612823666170316124500
8. Quail DF, Joyce JA. The microenvironmental landscape of brain tumors. *Cancer Cell*. (2017) 31:326–41. doi: 10.1016/j.ccell.2017.02.009
9. Gupta N, Shyamasundar S, Patnala R, Karthikeyan A, Arumugam TV, Ling EA, et al. Recent progress in therapeutic strategies for microglia-mediated neuroinflammation in neuropathologies. *Expert Opin Ther Targets*. (2018) 22:765–81. doi: 10.1080/14728222.2018.1515917
10. Baecher-Allan C, Kaskow BJ, Weiner HL. Multiple sclerosis: mechanisms and immunotherapy. *Neuron*. (2018) 97:742–68. doi: 10.1016/j.neuron.2018.01.021
11. Pitteri M, Magliozzi R, Bajrami A, Camera V, Calabrese M. Potential neuroprotective effect of Fingolimod in multiple sclerosis and its association with clinical variables. *Expert Opin Pharmacother*. (2018) 19:387–95. doi: 10.1080/14656566.2018.1434143
12. von Glehn F, Dias-Carneiro RPC, Moraes AS, Farias AS, Silva VAPG, Oliveira FTM, et al. Dimethyl fumarate downregulates the immune response through the HCA2/GPR109A pathway: implications for the treatment of multiple sclerosis. *Mult Scler Relat Disord*. (2018) 23:46–50. doi: 10.1016/j.msard.2018.04.016
13. Edmonds Y, Milstien S, Spiegel S. Development of small-molecule inhibitors of sphingosine-1-phosphate signaling. *Pharmacol Ther*. (2011) 132:352–60. doi: 10.1016/j.pharmthera.2011.08.004
14. Payne SG, Milstien S, Barbour SE, Spiegel S. Modulation of adaptive immune responses by sphingosine-1-phosphate. *Semin Cell Dev Biol*. (2004) 15:521–7. doi: 10.1016/j.semcdb.2004.05.008
15. Booth L, Cruickshanks N, Tavallai S, Roberts JL, Peery M, Poklepovic A, et al. Regulation of dimethyl-fumarate toxicity by proteasome inhibitors. *Cancer Biol Ther*. (2014) 15:1646–57. doi: 10.4161/15384047.2014.967992
16. Bennett Saidu NE, Bretagne M, Mansuet AL, Just PA, Leroy K, Cerles O, et al. Dimethyl fumarate is highly cytotoxic in KRAS mutated cancer cells but spares non-tumorigenic cells. *Oncotarget*. (2018) 9:9088–99. doi: 10.18632/oncotarget.24144
17. Georgakopoulos ND, Frison M, Alvarez MS, Bertrand H, Wells G, Campanella M. Reversible Keap1 inhibitors are preferential pharmacological tools to modulate cellular mitophagy. *Sci Rep*. (2017) 7:10303. doi: 10.1038/s41598-017-07679-7
18. Gillard GO, Collette B, Anderson J, Chao J, Scannevin RH, Huss DJ, et al. DMF, but not other fumarates, inhibits NF- κ B activity *in vitro* in an Nrf2-independent manner. *J Neuroimmunol*. (2015) 283:74–85. doi: 10.1016/j.jneuroim.2015.04.006
19. Peng H, Li H, Sheehy A, Cullen P, Allaire N, Scannevin RH. Dimethyl fumarate alters microglia phenotype and protects neurons against proinflammatory toxic microenvironments. *J Neuroimmunol*. (2016) 299:35–44. doi: 10.1016/j.jneuroim.2016.08.006
20. Booth L, Roberts JL, Poklepovic A, Avogadri-Connors F, Cutler RE, Lalani AS, et al. HDAC inhibitors enhance neratinib activity and when combined enhance the actions of an anti-PD-1 immunomodulatory antibody *in vivo*. *Oncotarget*. (2017) 8:90262–77. doi: 10.18632/oncotarget.21660
21. Booth L, Roberts JL, Poklepovic A, Kirkwood J, Sander C, Avogadri-Connors F, et al. The levels of mutant K-RAS and mutant N-RAS are rapidly reduced in a Beclin1/ATG5 -dependent fashion by the irreversible ERBB1/2/4 inhibitor neratinib. *Cancer Biol Ther*. (2018) 19:132–7. doi: 10.1080/15384047.2017.1394556
22. Booth L, Roberts JL, Rais R, Kirkwood J, Avogadri-Connors F, Cutler RE Jr, et al. [Neratinib + Valproate] exposure permanently reduces ERBB1 and RAS expression in 4T1 mammary tumors and enhances M1 macrophage infiltration. *Oncotarget*. (2017) 9:6062–74. doi: 10.18632/oncotarget.23681
23. Booth L, Roberts JL, Rais R, Cutler RE Jr, Diale I, Lalani AS, et al. Palbociclib augments Neratinib killing of tumor cells that is further enhanced by HDAC inhibition. *Cancer Biol Ther*. (2018) 5:1–12. doi: 10.1080/15384047.2018.1507665
24. Booth L, Roberts JL, Rais R, Cutler RE Jr, Diale I, Lalani AS, et al. Neratinib augments the lethality of [regorafenib + sildenafil]. *J Cell Physiol*. (2019) 234:4874–87. doi: 10.1002/jcp.27276
25. Booth L, Roberts JL, Cruickshanks N, Grant S, Poklepovic A, Dent P. Regulation of OSU-03012 toxicity by ER stress proteins and ER stress-inducing drugs. *Mol Cancer Ther*. (2014) 13:2384–98. doi: 10.1158/1535-7163.MCT-14-0172
26. Booth L, Roberts JL, Cruickshanks N, Tavallai S, Webb T, Samuel P, et al. PDE5 inhibitors enhance celecoxib killing in multiple tumor types. *J Cell Physiol*. (2015) 230:1115–27. doi: 10.1002/jcp.24843
27. Yacoub A, Mitchell C, Hong Y, Gopalkrishnan RV, Su ZZ, Gupta P, et al. MDA-7 regulates cell growth and radiosensitivity *in vitro* of primary (non-established) human glioma cells. *Cancer Biol Ther*. (2004) 3:739–51. doi: 10.4161/cbt.3.8.968
28. Dent P, Booth L, Poklepovic A, Hancock JF. Signaling alterations caused by drugs and autophagy. *Cell Signal*. (2019) 64:109416. doi: 10.1016/j.cellsig.2019.109416
29. Booth LA, Roberts JL, Dent P. The role of cell signaling in the crosstalk between autophagy and apoptosis in the regulation of tumor cell survival in response to sorafenib and neratinib. *Semin Cancer Biol*. (2019). doi: 10.1016/j.semcancer.2019.10.013. [Epub ahead of print].
30. Booth L, Poklepovic A, Dent P. Not the comfy chair! Cancer drugs that act against multiple active sites. *Expert Opin Ther Targets*. (2019) 23:893–901. doi: 10.1080/14728222.2019.1691526
31. Dent P, Booth L, Roberts JL, Liu J, Poklepovic A, Lalani AS, et al. Neratinib inhibits Hippo/YAP signaling, reduces mutant K-RAS expression, and kills pancreatic and blood cancer cells. *Oncogene*. (2019) 38:5890–904. doi: 10.1038/s41388-019-0849-8
32. Tripathi DN, Chowdhury R, Trudel LJ, Tee AR, Slack RS, Walker CL, et al. Reactive nitrogen species regulate autophagy through ATM-AMPK-TSC2-mediated suppression of mTORC1. *Proc Natl Acad Sci USA*. (2013) 110:E2950–7. doi: 10.1073/pnas.1307736110
33. Park MA, Mitchell C, Zhang G, Yacoub A, Allegood J, Häussinger D, et al. Vorinostat and sorafenib increase CD95 activation in gastrointestinal tumor cells through a Ca(2+)-*de novo* ceramide-PP2A-reactive oxygen species-dependent signaling pathway. *Cancer Res*. (2010) 70:6313–24. doi: 10.1158/0008-5472.CAN.10-0999
34. Guichet PO, Masliantsev K, Tachon G, Petropoulos C, Godet J, Larrieu D, et al. Fatal correlation between YAP1 expression and glioma aggressiveness: clinical and molecular evidence. *J Pathol*. (2018) 246:205–16. doi: 10.1002/path.5133
35. Artinian N, Cloninger C, Holmes B, Benavides-Serrato A, Bashir T, Gera J. Phosphorylation of the hippo pathway component AMOTL2 by the mTORC2 kinase promotes YAP signaling, resulting in enhanced glioblastoma growth and invasiveness. *J Biol Chem*. (2015) 290:19387–401. doi: 10.1074/jbc.M115.656587
36. Lee H, Hwang SJ, Kim HR, Shin CH, Choi KH, Joung JG, et al. Neurofibromatosis 2 (NF2) controls the invasiveness of glioblastoma through YAP-dependent expression of CYR61/CCN1 and miR-296-3p. *Biochim Biophys Acta*. (2016) 1859:599–611. doi: 10.1016/j.bbagr.2016.02.010
37. Wong SW, Sil P, Martinez J. Rubicon: LC3-associated phagocytosis and beyond. *FEBS J*. (2018) 285:1379–88. doi: 10.1111/febs.14354
38. Martinez J, Malireddi RK, Lu Q, Cunha LD, Pelletier S, Gingras S, et al. Molecular characterization of LC3-associated phagocytosis reveals distinct roles for Rubicon, NOX2 and autophagy proteins. *Nat Cell Biol*. (2015) 17:893–906. doi: 10.1038/ncb3192
39. Qiao L, Studer E, Leach K, McKinstry R, Gupta S, Decker R, et al. Deoxycholic acid (DCA) causes ligand-independent activation of epidermal growth factor receptor (EGFR) and FAS receptor in primary hepatocytes: inhibition of EGFR/mitogen-activated protein kinase-signaling module enhances DCA-induced apoptosis. *Mol Biol Cell*. (2001) 12:2629–45. doi: 10.1091/mbc.12.9.2629
40. Delos Santos RC, Garay C, Antonescu CN. Charming neighborhoods on the cell surface: plasma membrane microdomains regulate receptor tyrosine kinase signaling. *Cell Signal*. (2015) 27:1963–76. doi: 10.1016/j.cellsig.2015.07.004

41. Yu FX, Zhao B, Panupinthu N, Jewell JL, Lian I, Wang LH, et al. Regulation of the Hippo-YAP pathway by G-protein-coupled receptor signaling. *Cell*. (2012) 150:780–91. doi: 10.1016/j.cell.2012.06.037
42. Cheng JC, Wang EY, Yi Y, Thakur A, Tsai SH, Hoodless PA. S1P stimulates proliferation by upregulating CTGF expression through S1PR2-mediated YAP activation. *Mol Cancer Res*. (2018) 16:1543–55. doi: 10.1158/1541-7786.MCR-17-0681
43. Buchroithner J, Erhart F, Pichler J, Widhalm G, Preusser M, Stockhammer G, et al. Aducanumab immunotherapy based on dendritic cells has no effect on overall and progression-free survival in newly diagnosed glioblastoma: a phase II randomized trial. *Cancers*. (2018) 10:E372. doi: 10.3390/cancers10100372
44. Reznik E, Smith AW, Taube S, Mann J, Yondorf MZ, Parashar B, et al. Radiation and immunotherapy in high-grade gliomas: where do we

stand? *Am J Clin Oncol*. (2018) 41:197–212. doi: 10.1097/COC.0000000000000406

Conflict of Interest: The authors declare that the research was conducted in the absence of any commercial or financial relationships that could be construed as a potential conflict of interest.

Copyright © 2020 Dent, Booth, Roberts, Poklepovic and Hancock. This is an open-access article distributed under the terms of the Creative Commons Attribution License (CC BY). The use, distribution or reproduction in other forums is permitted, provided the original author(s) and the copyright owner(s) are credited and that the original publication in this journal is cited, in accordance with accepted academic practice. No use, distribution or reproduction is permitted which does not comply with these terms.